Supplementary materials

Text S1 Response surface methodology (RSM) design

Response surface methodology (RSM) was used to optimize the preparation conditions of modified sludge-derived biochar for enhanced the adsorption performance. In this study, a Box-Behnken design was implemented using Design-Expert 13 software. The independent variables selected were final pyrolysis temperature (A), pyrolysis time (B), and modification ratio ($CaCl_2$/sludge, C). The encoding scheme and levels for independent variables are presented in Table S1. The adsorption capacity was chosen as the response variable. The central point experiment was repeated 5 times, and the RSM design scheme and experimental results were shown in Table S2. A second-degree polynomial model was fitted to the experimental data. The significance and reliability of the model was evaluated using analysis of variance (ANOVA) and diagnostic plots. The resulting quadratic model was shown below:

$$Q = 18.23 + 2.73A + 0.1825B + 3.38C - 0.0050AB + 0.6600AC + 0.1900BC - 1.46A^2 - 0.4070B^2 - 0.2870C^2 \quad \text{(S1)}$$

In this equation, A, B and C represent the coded values for final pyrolysis temperature, pyrolysis time, and modification ratio, respectively.

The ANOVA for the RSM model (Table S3) implied the high significance of the model, as indicated by the low p value ($p = 0.0012$) and the high F value ($F = 13.37$). Furthermore, the high determination coefficient ($R^2 = 0.9450$) and the adequate signal-to-noise ratio (13.6595>4) indicated the good correlation and rationality of the model. Figure S1(a) and (b) depicted the normal distribution test of externally studentized residuals and the residual distribution of predicted values, respectively. The residuals conformed to the assumption of normal distribution and the predicted value residuals were randomly distributed, indicating the good applicability of the model.

The 3D response surfaces in Figure S1(c)–(e), generated by holding the third variable at its central level, illustrate the interactions between factors. The response surface for the final pyrolysis temperature and modification ratio (Fig. S1(d)) was steep, indicating these two parameters exerted the strong influence on adsorption capacity. Conversely, the response surfaces involving pyrolysis time were relatively flat, with only a slight bend observed, indicating the limited effects of pyrolysis time on adsorption capacity.

The quadratic model predicted an optimal preparation scheme of 800 °C, 2 h,

and a 0.90 g $CaCl_2$/g sludge ratio, yielding a maximum capacity of 23.26 mg/g. However, the experimental value for this condition was 22.36 ± 0.31 mg/g, slightly lower than the prediction. Considering this result and the minor influence of pyrolysis time on adsorption capacity, two optimal preparations were selected for this study: (1) CaSBC800 (22.36±0.31 mg/g): 0.90 g $CaCl_2$/g sludge, 800℃ and 2 h; (2) CaSBC600 (22.19±0.25 mg/g): 0.90 g $CaCl_2$/g sludge, 600℃ and 3 h.

Text S2 Batch experiment design

Adsorption experiments were conducted in 100 mL conical flasks containing 50 mL of solution, and the dosage of adsorbent was controlled at 1 g/L. The specific parameters for the kinetic, isotherm and environmental factor effect experiments were as follows.

Kinetic experiments were conducted with an initial SMX concentration of 5 mg/L and a solution pH of 7. The samples were shaken at 298 K and collected at different reaction time (0.033, 0.083, 0.17, 0.5, 1, 2, 4, 6, 8 and 12 h). The obtained data were fitted to pseudo-first order, pseudo-second order, Elovich, and intra-particle diffusion kinetic models (Table S5).

Isotherm experiments were performed at different initial SMX concentrations of 1, 5, 10, 20, 30, 40 and 50 mg/L at pH 7. To evaluate thermodynamic characteristics of adsorption process, isotherms were determined at 15, 25, 35 and 45 ℃. The data were fitted to the Langmuir and Freundlich isotherm models (Table S5) and the superior fit was used for adsorption site energy analysis.

Environmental factor experiments investigated the effects of pH, co-existing ions, and humic acid (HA) at the initial SMX concentration of 5 mg/L. pH experiments were conducted with initial pH values of 2, 4, 6, 8, 10 and 12. The influence of coexisting ions (Ca^{2+}, NH_4^+, SO_4^{2-}, NO_3^-, $H_2PO_4^-$, and HCO_3^-) was examined by adding 0–10 (0, 0.1, 0.5, 1, 5 and 10) mmol/L of each ion at pH 7. The effect of HA was tested at concentrations of 0–50 (0, 1, 5, 10, 20 and 50) mg/L at pH 7. All environmental factor experiments were agitated at 298 K for 12 h, maintaining other conditions constant.

Text S3 Calculation of production cost of CaSBC600 and SBC600

A simplified production cost was estimated for 1 kg of CaSBC600. The total cost was derived by summing the baseline cost of activated carbon (AC), \$1.38/kg, and all incremental costs associated with the modification process. These include material procurement ($CaCl_2$, HCl), process energy, wastewater treatment, and operational overheads (e.g., labor). Detailed calculations are as follows:

1. Cost of $CaCl_2$: 2.5 kg dried sludge is required to produce 1 kg CaSBC600 (based on a 40% yield) and the proportion of modification is set as 0.9 g $CaCl_2$/g sludge. The industrial-grade $CaCl_2$ price is ~\$179.46/ton, thus the cost from preparing $CaCl_2$ is \$0.40/kg CaSBC600.

2. Process energy: The impregnation is performed at a solid-liquid ratio of 1:10. Assuming that it requires to heat 25 kg water from 20 ℃ to 60 ℃, it totally needs 4200 kJ energy (1.16 kWh). The industrial electricity price in China is ~\$0.086/kWh. Therefore, the electricity cost is about \$0.10/kg CaSBC600.

3. Cost of HCl: After pyrolysis (yield 70%), the materials need to be washed with 1 mol/L HCl (solid/liquid ration = 1:10). 1.46 kg concentrated hydrochloric acid is required. The price of industrial concentrated hydrochloric acid is ~\$39.34/ton. Therefore, the cost from preparing HCl is \$0.06/kg CaSBC600.

4. Cost for wastewater treatment: The entire production process generates ~77.5 kg wastewater/kg CaSBC600, including 25 kg impregnation solution and 52.5 kg acid washing solution (wash with twice the volume of deionized water). The average sewage treatment fee for non-residential water is \$0.21/m^3. Therefore, wastewater treatment costs \$0.16/kg CaSBC600.

5. Operational overheads: Other operational costs (e.g., labor) are conservatively estimated at 20% of the sum of the above computable costs.

Therefore, the total estimated production cost for 1 kg of CaSBC600 is \$2.26.

For 1 kg SBC600, the incremental costs generated by cleaning, including material procurement (HCl), wastewater treatment, and operational overheads (e.g., labor). The costs estimated for each part are as follows:

1. Cost of HCl: 2 kg dried sludge is required to produce 1 kg CaSBC600 (yield 50%). After pyrolysis (yield 70%), the materials need to be washed with 1 mol/L HCl (solid/liquid ration=1:10). 1.17 kg concentrated hydrochloric acid is required. The price of industrial concentrated hydrochloric acid is ~\$39.34/ton, thus the cost from

preparing HCl is $0.05/kg CaSBC600.

2. Cost for wastewater treatment: The entire production process generates ~42 kg wastewater/kg SBC600 (wash with twice the volume of deionized water after acid washing). The average sewage treatment fee for non-residential water is $0.21/$m^3$. Therefore, wastewater treatment costs $0.09/kg SBC600.

3. Operational overheads: Other operational costs (e.g., labor) are conservatively estimated at 20% of the sum of the above computable costs.

Therefore, the total estimated production cost for 1 kg of SBC600 is $1.82.

Table S1 Elemental composition of the raw sludge.

Element	Content (wt%)
C	20.6
N	2.1
H	1.4
O	20.0

Table S2 The independent variable encoding and factor level of Box-Behnken model.

Variable	Unit	Factor	Coded value		
			–1	0	1
Temperature	℃	A	400	600	800
Time	h	B	1	2	3
Ratio	g/g	C	0.1	0.5	0.9

Table S3 ANOVA for quadratic model of adsorption capacity.

Source	Sum of squares	Degree of freedom	Mean square	F value	*p* value
Model	163.79	9	18.19	13.37	0.0012**
A-final pyrolysis temperature	59.84	1	59.84	43.98	0.0003***
B- pyrolysis time	0.2664	1	0.2664	0.1958	0.6715
C-modification ratio	91.12	1	91.12	66.97	<0.0001****
AB	0.0001	1	0.0001	0.0001	0.9934
AC	1.74	1	1.74	1.28	0.2951
BC	0.1444	1	0.1444	0.1061	0.7541
A^2	8.94	1	8.94	6.57	0.0374*
B^2	0.6975	1	0.6975	0.5126	0.4972
C^2	0.3468	1	0.3468	0.2549	0.6292
Residual	9.52	7	1.36		
Pure error	2.1	4	0.5242		
Cor total	173.22	16			

Note: *(p<0.05), **(p<0.01), ***(p<0.001), ****(p<0.0001) represented the significance degree of difference.

Table S4 RSM design scheme and experimental results.

Number	A: final pyrolysis temperature (℃)	B: pyrolysis time (h)	C: modification ratio (g/g)	Q: adsorption capacity (mg/g)
1	400	1	0.5	13.45
2	800	1	0.5	18.81
3	400	3	0.5	13.94
4	800	3	0.5	19.28
5	400	2	0.1	11.94
6	800	2	0.1	16.21
7	400	2	0.9	15.45
8	800	2	0.9	22.36
9	600	1	0.1	13.27
10	600	3	0.1	13.14
11	600	1	0.9	21.56
12	600	3	0.9	22.19
13	600	2	0.5	17.73
14	600	2	0.5	17.80
15	600	2	0.5	19.49
16	600	2	0.5	17.96
17	600	2	0.5	18.19

Table S5 Analytical formulas and models.

Type	Model	Mathematical expressions	Parameters
Formulas	Removal rate	$R = \frac{C_0 - C_t}{C_0} \times 100\%$	R (%): removal rate of SMX; C_0 (mg/L): initial concentration of SMX; C_t (mg/L): concentration of SMX at time t (min).
	Adsorption capacity	$q = \frac{V(C_0 - C_t)}{m}$	q (mg/g): adsorption capacity of SMX; V (L): volume of the reaction solution; m (g): quality of the adsorbent.
	Thermodynamics	$K_T = \frac{q_e}{C_e}$ $\Delta G = -RT \ln K_T = \Delta H - T\Delta S$ $\ln K_T = \frac{\Delta S}{R} - \frac{\Delta H}{RT}$	q_e (mg/g): equilibrium adsorption capacity; C_e (mg/L): equilibrium concentration of SMX; K_T (L/g): adsorption equilibrium constant; T (K): reaction temperature; ΔG (J/mol): Gibbs free energy change; ΔH (J/mol): enthalpy change; ΔS (J/(mol·K)): entropy change; R (8.314 J/(mol·K)): gas constant.
Kinetics	Pseudo first-order (PFO)	$q_t = q_e(1 - e^{-k_1 t})$	q_t (mg/g): adsorption capacity of SMX at time t (min); k_1 (min^{-1}): PFO kinetic rate constant.
	Pseudo second-order (PSO)	$q_t = \frac{q_e^2 k_2 t}{1 + q_e k_2 t}$	k_2 (min^{-1}): PSO kinetic rate constant.
	Elovich	$q_t = \frac{1}{\beta} \ln \alpha\beta + \frac{1}{\beta} \ln t = \frac{1}{\beta} \ln \alpha\beta t$	α (mg/(g·min)): Elovich initial rate constant; β (g/mg): Elovich rate constant, relating to desorption rate.
	Intra-particle diffusion	$q_t = Kt^{\frac{1}{2}} + C$	K [g/(mg·min$^{1/2}$)]: intra-particle diffusion rate constant; C: intra-particle diffusion constant, relating to boundary layer thickness.
Isotherm	Langmuir	$q_e = \frac{q_m C_e}{1/K_L + C_e}$	q_m (mg/g): maximum adsorption capacity; K_L (L/mg): Langmuir constant, relating to the adsorption energy.
	Freundlich	$q_e = K_F C_e^{1/n}$	K_F ((mg$^{1-1/n}$·L$^{1/n}$)/g): Freundlich constant, relating to adsorption capacity and intensity; n: a dimensionless constant, describing the degree of nonlinearity of the adsorption process.
Adsorption site energy	Based on Freundlich model	$F(E^*) = \frac{K_F C_S^{1/n}}{nRT} e^{-\frac{E^*}{nRT}}$ $\mu(E^*) = \frac{\int_{E_1^*}^{E_2^*} E^* \cdot F(E^*)\, dE^*}{\int_{E_1^*}^{E_2^*} F(E^*)\, dE^*}$ $\sigma^* = \sqrt{\mu[(E^*)^2] - [\mu(E^*)]^2}$	C_S (mg/L): solubility of adsorbate; $F(E^*)$ ((mg·mol)/(g·kJ)): site energy frequency distribution; E^* (kJ/mol): the difference between adsorption energies of the solute and solvent on the surface of the adsorbent; $\mu(E^*)$ (kJ/mol): average site energy; σ^* (kJ/mol): standard deviation, representing site energy heterogeneity.

Table S6 The specific surface area (SSA), pore volume and average pore diameter of adsorbents.

Adsorbent	SSA (m^2/g)	S_{Micro} (m^2/g)	V_{Pore} (cm^3/g)	V_{Micro} (cm^3/g)	D_{Pore} (nm)
CaSBC600	129.50	20.495	0.3015	0.0161	9.31
SBC600	101.22	8.5035	0.1611	0.0081	6.37
CaSBC800	139.63	21.227	0.3540	0.0169	10.14
SBC800	107.95	39.465	0.1803	0.0173	6.68
AC	153.01	121.52	0.1028	0.0619	2.69

Table S7 Comparison of SMX adsorption capacity on CaSBC with other adsorbents.

Adsorbents	Preparation conditions	Adsorption capacity (mg/g)	References
Modified sludge-derived biochar	$CaCl_2$ impregnation-pyrolysis (600℃) and subsequent acid washing	22.30 ± 0.74*	This work
Municipal sludge-derived biochar	Pyrolysis at 800°C	7.0334 (30°C)	(Qiu et al., 2023)
Chitosan-biochar composite derived from agricultural waste	spent coffee grounds biochar pyrolyzed at 600°C, modified by chitosan	14.73*	(Son Tran et al., 2023)
$FeCl_3$-activated bermudagrass (BG)-derived biochar	$FeCl_3$ impregnation-pyrolysis (800°C)	253*	(Zeng et al., 2021)
Ordered mesoporous carbon	Hard template approach using sucrose as the carbon precursor, carbonized at 900°C	334*	(Sarker et al., 2023)
Carbon doped boron nitride	One-step oxygen limiting method, heated at 500°C	28.750 (10°C) 22.700 (20°C) 19.075 (30°C)	(Sun et al., 2022)

* The adsorption was reacted at 25°C.

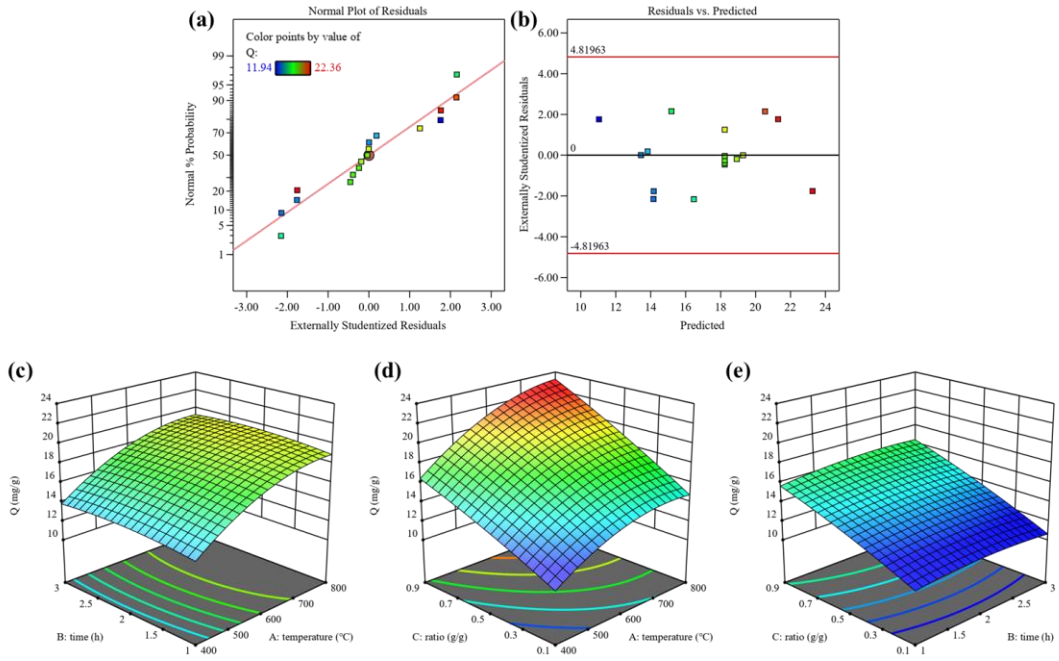

Fig. S1 (a) Externally studentized residual normal distribution test; (b) Residual analysis of predicted value; (c–e) 3D response surface of interaction.

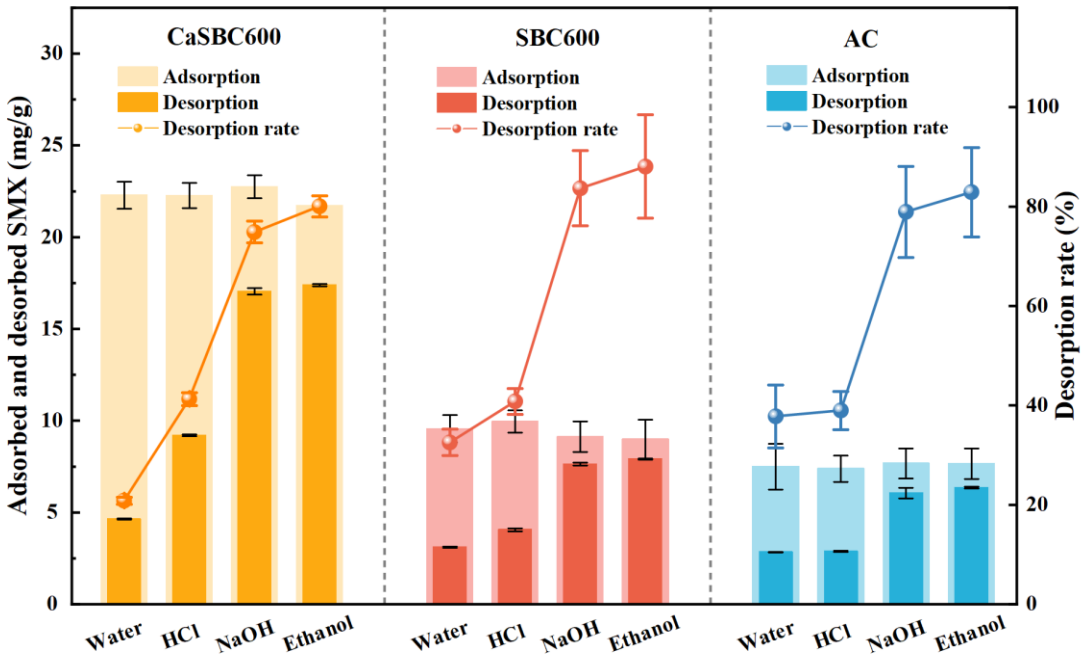

Fig. S2 The elution-desorption performance of the adsorbents. Reaction conditions: dosage of adsorbent = 1g/L, SMX concentration = 50 mg/L, pH = 7, temperature = 25℃, eluent concentration (HCl/NaOH) = 0.1 mol/L.

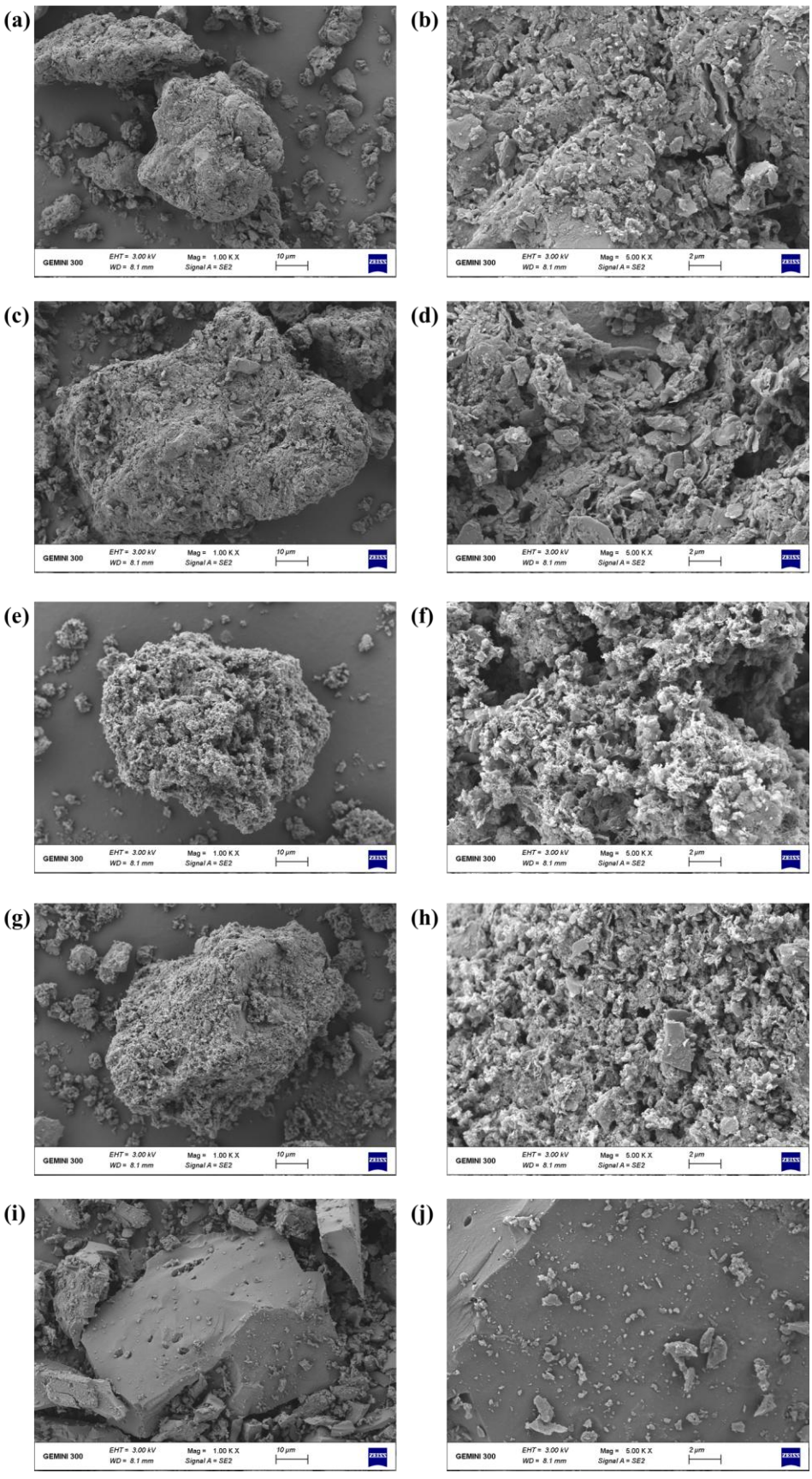

Fig. S3 SEM images of sludge-derived biochar: (a–b) SBC600; (c–d) SBC800; (e–f) CaSBC600; (g–h) CaSBC800; (i–j) Activated carbon.

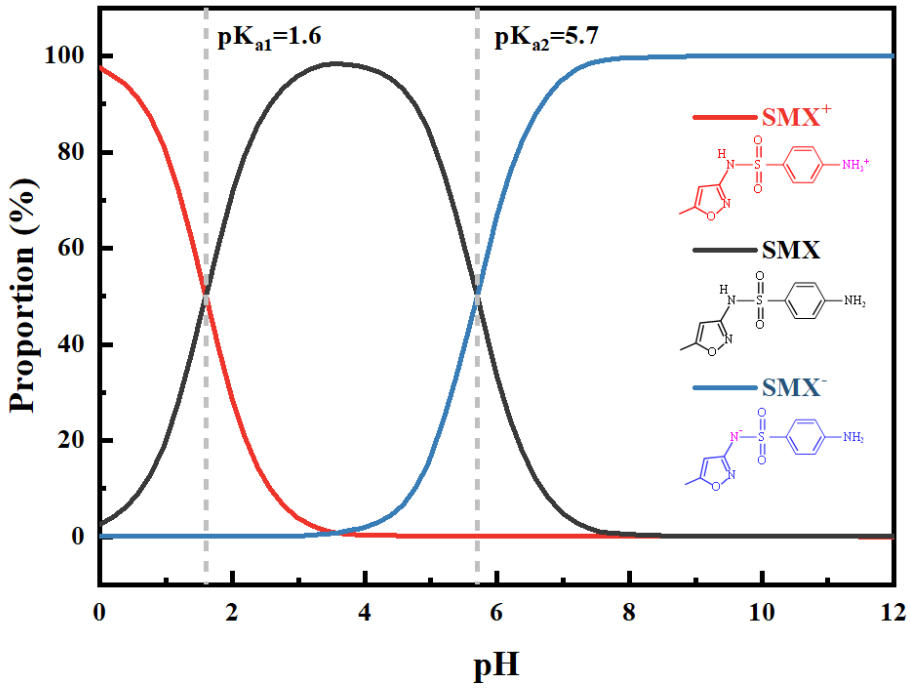

Fig. S4 The dissociation curve of SMX.

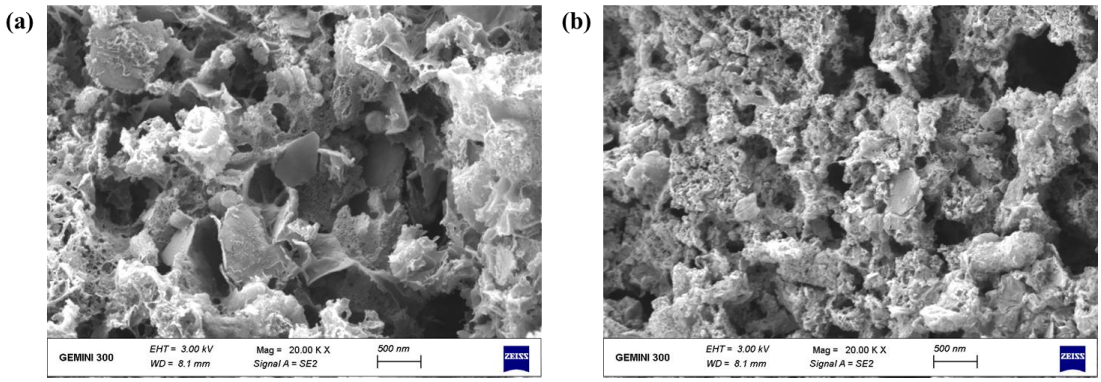

Fig. S5 SEM images of CaSBC600: (a) before adsorption; (b) after adsorption.

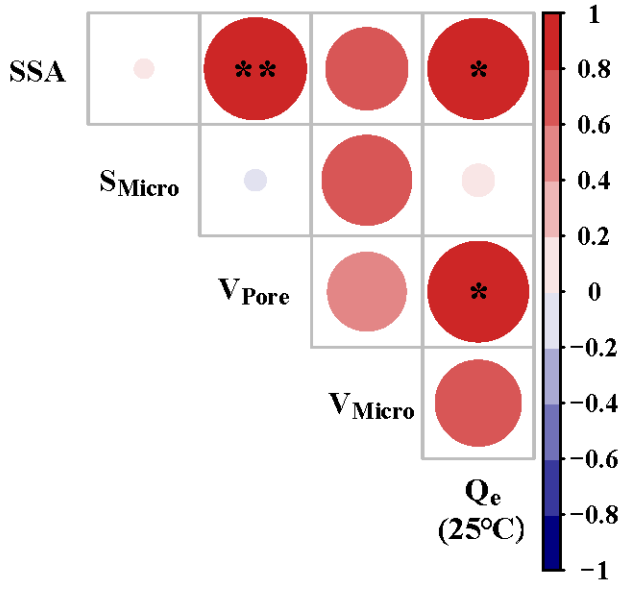

Fig. S6 Correlation between physical properties and adsorption performance ("*" and "" stand for $p<0.05$ and $p<0.01$ respectively).**

References

Diao Y, Shan R, Li M, Gu J, Yuan H, Chen Y (2023). Efficient Adsorption of a Sulfonamide Antibiotic in Aqueous Solutions with N-doped Magnetic Biochar: Performance, Mechanism, and Reusability. ACS Omega. 8(1): 879–892. doi:10.1021/acsomega.2c06234.

Ninwiwek N, Hongsawat P, Punyapalakul P, Prarat P (2019). Removal of the antibiotic sulfamethoxazole from environmental water by mesoporous Silica-magnetic graphene oxide nanocomposite technology: Adsorption characteristics, coadsorption and uptake Mechanism. Colloids and Surfaces A: Physicochemical and Engineering Aspects. 580: 123716. doi:10.1016/j.colsurfa.2019.123716.

Qiu X, Zhao Y, Zhao C, Jin R, Li C, Mutabazi E (2023). Physicochemical and adsorptive properties of biochar derived from municipal sludge: Sulfamethoxazole adsorption and underlying Mechanism. Frontiers in Environmental Science. 11: 1275087. doi:10.3389/fenvs.2023.1275087.

Sarker P, Lei X, Taylor K, Holmes W, Yan H, Cao D, Zappi M E, Gang D D (2023). Evaluation of the adsorption of sulfamethoxazole (SMX) within aqueous influents onto customized ordered mesoporous carbon (OMC) adsorbents: Performance and elucidation of key adsorption Mechanisms. Chemical Engineering Journal. 454: 140082. doi:10.1016/j.cej.2022.140082.

Son Tran V, Hao Ngo H, Guo W, Ha Nguyen T, Mai Ly Luong T, Huan Nguyen X, Lan Anh Phan T, Trong Le V, Phuong Nguyen M, Khai Nguyen M (2023). New Chitosan-biochar composite derived from agricultural waste for removing sulfamethoxazole antibiotics in Water. Bioresource Technology. 385: 129384. doi:10.1016/j.biortech.2023.129384.

Sun Y, Bian J, Zhu Q (2022). Sulfamethoxazole removal of adsorption by carbon – Doped boron nitride in Water. Journal of Molecular Liquids. 349: 118216. doi:10.1016/j.molliq.2021.118216.

Zeng S, Kan E (2022). Sustainable use of $Ca(OH)_2$ modified biochar for phosphorus recovery and tetracycline removal from Water. Science of The Total Environment. 839: 156159. doi:10.1016/j.scitotenv.2022.156159.